NASA Technical Memorandum 83295

TIME-MARCHING TRANSONIC FLUTTER SOLUTIONS INCLUDING ANGLE-OF-ATTACK EFFECTS

JOHN W. EDWARDS, ROBERT M. BENNETT,
WOODROW WHITLOW, JR. AND DAVID A. SEIDEL

APRIL 1982

National Aeronautics and
Space Administration

Langley Research Center
Hampton, Virginia 23665

TIME-MARCHING TRANSONIC FLUTTER SOLUTIONS INCLUDING ANGLE-OF-ATTACK EFFECTS

John W. Edwards, Robert M. Bennett, Woodrow Whitlow, Jr., and David A. Seidel†
NASA Langley Research Center
Hampton, Virginia 23665

Abstract

Transonic aeroelastic solutions based upon the transonic small perturbation potential equation are studied. Time-marching transient solutions of plunging and pitching airfoils are analyzed using a complex exponential modal identification technique, and seven alternative integration techniques for the structural equations are evaluated. The HYTRAN2 code is used to determine transonic flutter boundaries versus Mach number and angle-of-attack for NACA 64A010 and MBB A-3 airfoils. In that code, a monotone differencing method, which eliminates leading edge expansion shocks, is used to solve the potential equation. When the effect of static pitching moment upon the angle-of-attack is included, the MBB A-3 airfoil can have multiple flutter speeds at a given Mach number.

Nomenclature

a	nondimensional elastic axis location, measured from midchord
a_i	amplitude of ith mode, eq. (10)
A,B	(4x4) and (4x2) matrices, eq. (4)
b	airfoil semichord, m.
c_ℓ	nondimensional lift coefficient, positive downwards
c_m	nondimensional moment coefficient about a, positive nose up
C_p	nondimensional pressure coefficient
$f(x,t)$	airfoil shape function
h	nondimensional plunge displacement of elastic axis, positive downwards
I	identity matrix
j	$\sqrt{-1}$
k	reduced frequency, $\omega b/U$
k_α	pitch spring constant
m	airfoil mass per unit span
M	Mach number
M,K,B'	(2x2) mass, stiffness, and input matrices, eq. (3)
r_α	radius of gyration about elastic axis
$s_i=\sigma_i+j\omega_i$	Laplace transform variable, rad/sec
t,τ	time, sec
T	integration step size, sec
U	airspeed, m/sec
u	(2x1) airload vector, eq. (3)
V	speed index, $U/b\omega_\alpha\sqrt{\mu}$
x,z	cartesian coordinates
$\underline{x}$	(4x1) state vector, eq. (4)
x_α	dimensionless static unbalance
y	(2x1) mode vector, eq. (3)
α	angle-of-attack, rad. (deg.)
γ	ratio of specific heats
$\zeta_i = \sigma_i/\omega_i$	damping ratio of ith mode
Ω	(4x4) matrix, integral of Φ
μ	airfoil mass ratio, $m/\pi\rho b^2$
ρ	fluid density, kg/m^3
ψ_i	phase of ith mode, eq. (10)
ϕ	velocity potential
Φ	(4x4) state transition matrix
ω_h,ω_α	uncoupled plunge and pitch mode frequencies, rad/sec

superscripts

T	transpose
$\cdot$	time derivative

subscripts

i	index
n	time step index
o	initial or steady condition
∞	freestream

Introduction

The calculation of aeroelastic response characteristics in the transonic speed range is of much current interest since the avoidance of transonic flutter is a key design problem. Prior to the development of computer programs capable of solving transonic aerodynamic problems, linear subsonic and supersonic solutions were extended into this regime even though the assumptions of the underlying theory were violated. The LTRAN2[1] computer program solves the two-dimensional, low frequency, transonic, small perturbation potential equation. Its application to a simple aeroelastic stability problem was demonstrated by Ballhaus and Goorjian.[2] Ref. 2 illustrates the two approaches which have been followed in the application of transonic aerodynamic calculations to aeroelasticity; namely, harmonic analysis and time-marching analysis. The former assumes that the unsteady aerodynamic forces are locally linear and utilizes traditional modal superposition of harmonic loads while the latter delays the question of linearity by calculating the transient response of the coupled aerodynamic-structural system. If the assumption of local linearity is warranted, the harmonic analysis approach offers a significant computational savings. Rizzetta[3] examined the time-marching technique, using a four-point Adams-Moulton integrator for the structural equations of motion and the LTRAN2 code to calculate the unsteady airloads. The initial conditions chosen were large enough that significant nonlinear effects occurred in the calculated unsteady airloads, indicating large shock motions. Yang, Guruswamy, and Striz[4] studied a time-marching scheme which coupled transient LTRAN2 solutions and a structural integrator which assumed a linear variation of velocities. They also compared harmonic flutter analyses[5] using oscillatory airloads derived from LTRAN2 and UTRANS2[6].

†Structures Engineer, Kentron International, Inc., Hampton, Virginia

Since the original LTRAN2 code is accurate only at low frequencies (k≤.075), several improvements were made to increase its range of applicability. Houwink and van der Vooren[7] studied the effect of retaining the time derivative terms in the boundary and auxiliary conditions in their LTRAN2-NLR code and claimed accuracy to k = 0.4. Rizzetta and Chin[8] retained, in addition, the high frequency (ϕ_{tt}) term in the governing equation. Isogai[9] has included both of these effects in a computer code which has been used to generate oscillatory airloads for a harmonic flutter analysis of a two-dimensional airfoil section. The analysis demonstrated a significant transonic dip in the section's flutter boundary. Borland and Rizzetta[10] have developed a three-dimensional unsteady aerodynamic code, XTRAN3S, and have utilized a centered difference structural integration technique to obtain transient time-marching flutter solutions.

Application of these time dependent small-perturbation codes has been hampered by numerical stability problems which occur for large amplitude motion and/or large angles-of-attack. The current study modifies the LTRAN2-NLR code with the monotone differencing scheme of Engquist and Osher[11] in order to eliminate the source of this problem, namely expansion shocks near the airfoil leading-edge. The resulting code is termed HYTRAN2. This code has been used to study the accuracy and stability of the various numerical integration techniques which may be used in transient time-marching calculations. The accuracy of the finite-difference computer program algorithms may be established using recent analytic solutions by Bland[12] of the linearized LTRAN2, HYTRAN2, and EXTRAN2 aerodynamic problems. The linearized version of the HYTRAN2 code is then used to investigate the accuracy of various numerical integration techniques for the structural equations of motion. A comparison is made of transonic flutter boundaries of the NACA 64A010 airfoil calculated by four different nonlinear transonic codes. The effect of angle-of-attack upon the flutter boundaries of the NACA 64A010 and the MBB A-3 airfoils is also demonstrated. Finally, the effect upon the flutter boundary of including the aeroelastic twisting resulting from the steady pitching moment is demonstrated.

Unsteady Transonic Small Perturbation Equation

The calculations described herein were obtained from a modified version of the LTRAN2-NLR code[7] which solves the low frequency transonic small perturbation (TSP) potential equation

$$[1-M_\infty^2-(\gamma^*+1)M_\infty^2\phi_x]\,\phi_{xx} + \phi_{zz} - 2M_\infty^2\,\phi_{xt} = 0 \qquad (1)$$

subject to the following airfoil boundary and wake conditions

$$\phi_z = f_x + f_t;\ z = \pm 0,\ 0 < x < 1 \qquad (2a)$$

$$[\phi_x] + [\phi_t] = 0;\ z = 0,\ x>1 \qquad (2b)$$

Aerodynamic loads are given in terms of a nondimensional pressure coefficient, C_p, which in the small perturbation limit becomes

$$C_p = -2(\phi_x + \phi_t) \qquad (2c)$$

The airfoil coordinates are given by $z = f(x,t)$, and $\gamma^* = 2-(2-\gamma)M_\infty^2$. The original LTRAN2[1] grid of 99 by 79 points in the x and z direction, respectively, with 33 points on the airfoil chord was used. The original LTRAN2-NLR and LTRAN2 codes are very sensitive to angle-of-attack changes and large airfoil pitching or plunging motions, and numerical instabilities generated at the leading edge[13] can lead to program failure. The monotone differencing method of Engquist and Osher[11] eliminates the leading edge expansion shocks which cause this problem and has been incorporated into the code used for this study which is termed HYTRAN2. Solutions obtained with the time derivative terms of (2) deleted are referred to as LTRAN2 solutions while solutions with a $-M_\infty^2\phi_{tt}$ term added to (1) are referred to as EXTRAN2 solutions. Refs. 8 and 9 give results obtained from EXTRAN2 type codes.

The frequency limits of LTRAN2 and HYTRAN2 codes are generally accepted as k=0.075 and k=0.4 respectively. These estimates are based upon comparisons of results from linearized versions of these finite-difference codes (obtained by deleting the $\phi_x\phi_{xx}$ term in (1)) with classical solutions of the subsonic wave equation. This has left open the questions of convergence of solutions for a given grid and accuracy of the solutions. Bland[12] has modified the kernel function of the Possio integral equation to enable computation of exact analytic solutions of the LTRAN2 and HYTRAN2 linearized problems. Figure 1 gives comparisons of his exact c_{ℓ_α} solutions at M = 0.8 for the three different kernels with LTRAN2 and HYTRAN2 results for reduced frequencies up to 0.5. The finite-difference results were obtained using 3 cycles of time marching calculations with 360 steps per cycle. The agreement between the finite-difference and analytical solutions indicates that the finite-difference code is quite accurate for the grid and step size used. Also, the departure of LTRAN2 from the analytic EXTRAN2 results above k=0.05 confirms the limitations of LTRAN2 mentioned above. The HYTRAN2 results are in better agreement with EXTRAN2 and show a gradual departure from EXTRAN2. The selection of an upper frequency limit on HYTRAN2 is somewhat arbitrary.

Time-Marching Aeroelastic Solutions

The classical description of a two-dimensional, pitching and plunging airfoil is assumed. The airfoil lies between ±1 on the x-axis; plunge, h, and lift coefficient, c_ℓ are measured positive downwards at the elastic axis, a; and pitch, α, and moment coefficient about a, c_m, are positive nose up. The equations of motion are written in vector notation as

$$\ddot{y} = M^{-1}Ky + M^{-1}B'u \qquad (3)$$

where $y^T = [h\ \alpha]$, $u^T = [(c_\ell - c_{\ell_0})\ (c_m - c_{m_0})]$, and

$$M = \begin{bmatrix} 1 & x_\alpha \\ x_\alpha & r_\alpha^2 \end{bmatrix},\quad K = \begin{bmatrix} -\omega_h^2 & 0 \\ 0 & -r_\alpha^2\omega_\alpha^2 \end{bmatrix},$$

$$B' = \frac{\omega_\alpha^2}{\pi}\, V^2 \begin{bmatrix} 1 & 0 \\ 0 & 1 \end{bmatrix}$$

The static load coefficients, c_{ℓ_0} and c_{m_0}, are subtracted from the total coefficients during the time-marching calculation. Thus h and α represent perturbations about assumed static operating conditions. The static angle-of-attack is a separate input to HYTRAN2 and contributes to f_x in (2a). The speed index $V = U/b\omega_\alpha\sqrt{\mu}$ determines the density (altitude) assumed for a calculation. As V increases from zero, transient responses are initially damped. Further increases in V will usually lead to neutrally stable oscillations characterizing a flutter boundary. The value of V at flutter is termed the flutter speed index, V_f. A fourth order linear state equation may be developed from (3) as

$$\dot{x} = Ax + Bu \qquad (4)$$

where $x^T = [y^T\ \dot{y}^T] = [h\ \alpha\ \dot{h}\ \dot{\alpha}]$ and

$$A = \begin{bmatrix} 0 & I \\ M^{-1}K & 0 \end{bmatrix},\quad B = \begin{bmatrix} 0 \\ M^{-1}B' \end{bmatrix}$$

Structural Integration Technique

Published studies of time-marching aeroelastic solutions have coupled the structural equations of motion to aerodynamic codes using a variety of numerical integration techniques. Rizzetta[3] used an Adams-Moulton predictor-corrector scheme. Ref. 4 reports an algorithm based upon an assumed linear variation of acceleration while a centered-difference integration technique was used in ref. 10. None of these approaches takes advantage of the linear structure of (4).

Since (4) is a finite-dimensional linear differential equation, its solution[14] is

$$x(t) = \phi(t)x(0) + \int_0^t \exp[A(t-\tau)]Bu(\tau)\,d\tau \qquad (5)$$

The state transition matrix $\phi(t) = \exp[At]$ may be calculated to any desired accuracy as the sum of the first n terms of the series expansion of the matrix exponential function. The first term in (5) is the homogeneous response portion of (4) while the second term is a convolution integral giving the forced response. For use as a structural integrator in aeroelastic time marching solutions, (5) is rewritten to reflect the evolution of the structural state from time step n to time step n+1,

$$x[(n+1)T] = \phi(T)x(nT) + \int_{nT}^{(n+1)T} \exp[A((n+1)T-\tau)]Bu(\tau)\,d\tau \qquad (6)$$

where T is the step size.

The alternating-direction implicit solution algorithm used in HYTRAN2 requires three pieces of data to calculate the flow field potential, ϕ_{n+1}, at time step n+1: 1)ϕ_n, the potential at time n, 2)x_n, the boundary condition at time n, and 3)x_{n+1}, the boundary condition at time n+1. Since the lift and moment are not known over the interval $nT<t<(n+1)T$, the integral in (6) must be approximated. The simplest approximation is to assume that $u(t) = u(nT)$ over the interval. Then $\theta u(nT)$ may be taken out of the integral and a slight change of notation gives

$$x_{n+1} = \phi x_n + \theta u_n \qquad (7)$$

where the integral of the transition matrix is

$$\theta = \int_0^T \exp[A(T-\tau)]\,d\tau \qquad (8)$$

An improvement upon this approximation may be obtained by considering u to vary linearly between u_n and u_{n+1} in (6). Then, for small time steps, T, the integral is nearly equal to $\theta B(u_{n+1} + u_n)/2$. However, u_{n+1} is not available at this step of the algorithm and an estimate of $u_{n+1} = u_n + (u_n - u_{n-1})$ will be used. The resulting algorithm is

$$x_{n+1} = \phi x_n + \theta B(3u_n - u_{n-1})/2 \qquad (9)$$

The integration matrices φ and θ were calculated using the program described in ref. 15. Unless otherwise noted, the results presented were obtained from transient responses calculated using (9) for the structural integrator. After the steady state flow field for the static angle-of-attack was obtained the transient was excited by a one percent chord displacement initial condition on the plunge coordinate. The transient was calculated for 250 time steps which yielded 3-6 cycles of oscillation of the dominant flutter mode for the examples studied. To determine a flutter point, several transients were calculated for a range of speed indices, V. Typically, speed indices were used which gave slightly subcritical damped response and slightly supercritical diverging response. The flutter speed index was then determined by interpolation. Once the general nature of the flutter boundary was understood, additional flutter points could generally be obtained in this manner with the calculation of two responses per flutter point.

Section 3. Structural Parameters

The structural parameters for the two example cases studied are given in Table 1. Example 1 is the same as Case A of Isogai[9,16] which was selected to have plunging and pitching normal modes similar to those of a streamwise section near the wingtip of a sweptback wing. The pivotal point for the lowest frequency plunging mode is 1.44 chord lengths ahead of the leading-edge and for the higher frequency pitch mode it is 0.068 chordlengths ahead of midchord. Isogai[16] has shown a significant transonic dip in the flutter speed index of this section with the plunging mode becoming the flutter mode at frequencies ranging from 80-150 rad/sec.

Example 2 was chosen to investigate the situation in which the normal mode frequencies were close together and for which the higher frequency pitch mode would become the flutter mode. The small negative static unbalance leads to very little inertial coupling of the modes and also causes the section to be nearly statically unstable.

Table 1. SECTION STRUCTURAL PARAMETERS

	Example 1	Example 2
a	-2	-0.042
x_α	1.8	-0.036
r_α^2	3.48	1.872
μ	60	60
ω_h, r/s	100	23.5
ω_α, r/s	100	35
wind off plunge freq., r/s	71.34	23.497
wind off pitch freq., r/s	533.8	35.037

Modal Identification Technique

To efficiently use the information contained in the transients, the least squares curve fitting program of Bennett and Desmarais[17] was used. Both h and α responses were fit independently by the function

$$Y(t) = a_0 + \sum_{i=1}^{m} e^{-\sigma_i t} a_i \cos(\omega_i t + \psi_i) \qquad (10)$$

For the two degree-of-freedom examples treated m was set equal to two. The complex modes thus obtained, $s_i = \sigma_i + j\omega_i$, are estimates of the eigenvalues of the aeroelastic system and can be plotted as a function of speed index, V, giving s-plane root loci of the coupled plunge and pitch modes. Figure 2 gives a typical transient response of the MBB A-3 airfoil for Example 1 at M = 0.8 and an angle-of-attack $\alpha_0 = 0$. Shown at the top of figure are the h and α responses and the fits of the responses. At the bottom of the figure the time histories of the component modes of the fits are shown. The fits are very good and indicate that nonlinear effects are very small.

Table 2 gives the estimates of the two modes for each of two response time histories. Standard deviations of the estimates are computed from the residuals and are given in brackets beneath the estimates. The estimates given by the independent fits are very consistent with each other although the standard deviations are somewhat optimistic. These results indicate that locally linear techniques are applicable for this case involving plunging oscillations of $\pm$0.008 semichords and angle-of-attack oscillations of $\pm$0.25 deg.

TABLE 2. MODAL ESTIMATES FOR MBB A-3 RESPONSE AT M = 0.8 AND α_0 = 0 DEG.

	s_1, rad/sec	s_2, rad/sec
h-fit	-.12+j86.91 (.05+j .05)	-17.24+j535.54 (.31+j .32)
α-fit	-.02+j86.74 (.07+j .07)	-17.94+j536.81 (.42+j .43)

Airfoils

Figure 3 shows the profiles of the two airfoil studied. Coordinates for the NACA 64A010 symmetrical airfoil were taken from Abbott and von Doenhoff[18] and for the MBB A-3 supercritical airfoil from Bland.[19] Applications of TSP codes to both airfoils have been extensively reported (e.g. refs. 3, 8, 20, 21 for the NACA 64A010 and refs. 21, 22 for the MBB A-3). The MBB A-3 theoretical design condition is M = 0.765, α = 1.3 deg., and c_ℓ = 0.58 and experimental pressure distributions are given by Bucciantini et al[23]. The airfoil slopes required by HYTRAN2 were generated using the geometry processor of LTRAN2.[1]

The MBB A-3 slopes used in ref. 21 are from ref. 24 and were obtained from least-squares polynomial curve fits to airfoil ordinates. The resulting slopes are inaccurate, particularly for the leading-edge region of the upper surface and the trailing-edge region of the lower surface where the calculated pressures[21] are significantly different from experiment and design.[23] This problem has been corrected in ref. 22.

Linearized Aeroelastic Model

Pitching and plunging airload coefficients from Bland's exact solutions of the linearized LTRAN2, HYTRAN2, and EXTRAN2 problems were used to generate matrix Pade approximants of the loads using the technique described by Edwards.[25] The approximants were then available as linear differential equations which were

coupled to (4) to allow linear eigenvalue analysis of stability as a function of speed index. The approximants give a good approximation of the loads along the s-plane imaginary axis and, by analytic continuation, are also valid for complex values of s near the imaginary axis. These models, denoted PLTRAN2, PHYTRAN2, and PEXTRAN2, were used to evaluate time marching solutions from the linearized TSP equations for subcritical, critical and supercritical flutter conditions.

Results and Discussion

Comparison of Time-Marching and Linearized Solutions.

Aeroelastic root loci - Figure 4 compares the plunge and pitch mode root locations obtained from curve fits of the plunge response with root loci calculated using the linearized Pade models. The time-marching calculations were obtained from the linearized LTRAN2 and HTRAN2 codes using a flat plate airfoil. The Mach number is 0.8, and the Example 1 structural model was used with a time step of 0.001 sec. Time-marching results are shown for V = 0.87, 1.37, and 1.75 corresponding to flutter points of PLTRAN2, PEXTRAN2, and an unstable condition. These speed conditions for the Pade models are indicated by tick marks. The true flutter point for this case is given by PEXTRAN2 as V_f = 1.37, ω_f = 135 rad/sec, and k_f = 0.127 which is closely approximated by both the PHYTRAN2 and HYTRAN2 results. While the flutter point predicted for this case by PLTRAN2 at V_f = 0.87, ω_f = 101 rad/sec, and k_f = 0.15 is reasonably reproduced by the LTRAN2 result, both are over 35% low in V_f and significantly low in frequency. There is also good agreement between the time-marching results and the Pade model results for both the stable and unstable conditions. The pitch mode results do not show as good correspondence. This is due to: 1)The matrix Pade approximants are less accurate at the high reduced frequencies and damping ratios involved, and 2)time-marching integration errors are of concern for the relatively high pitch frequency of this example. Still, the HYTRAN2 results are in reasonable agreement with the PEXTRAN2 results. These results give confidence in the use of time-marching aeroelastic studies based upon the HYTRAN2 code.

Structural Equation Integrator Study - Table 3 lists seven integration techniques which may be used for the structural equations of motion. Each integrator was evaluated for its ability to accurately reproduce the PHYTRAN2 flutter point of fig. 4 as a function of time step size. Integrators I1 and I2 are the state transition matrix integrators of (7) and (9) while I3 is (9) implemented as a predictor-corrector. Integrator I4 is a centered difference (in time) algorithm based upon (4) while I5 is the centered difference algorithm used by Borland and Rizzetta[10] based upon (3). Integrator I6 has been used by Yang et al[21,22] while I7 is the same algorithm implemented as predictor-corrector and which was used in the XTRAN3S code.[26]

Table 4 gives the flutter (plunge) and pitch modes identified from the plunge transient responses of Example 1 at Mach 0.8 for step sizes of 0.0001-0.003 seconds and a speed index of V = 1.5. Table 5 gives the two modes identified from the plunge transient responses of Example 2 at Mach 0.8 for step sizes of 0.001-0.03 seconds and a speed index of V = 0.747. In this case the flutter root evolves from the higher frequency pitch mode. Also given are eigenvalues of the respective cases from PHYTRAN2 which are the "exact" values for the two flutter roots. This was ensured by forcing the matrix Pade approximants to match Bland's[12] exact load values at the respective flutter frequencies. The flutter reduced frequencies for the two examples of Tables 4 and 5 are k_f = 0.126 and 0.146, respectively.

TABLE 3. STRUCTURAL EQUATION INTEGRATORS

I1 $\underline{x}_{n+1} = \Phi \underline{x}_n + \Theta u_n$

I2 $\underline{x}_{n+1} = \Phi \underline{x}_n + .5\Theta[3u_n - u_{n-1}]$

I3 predictor; $\underline{x}_{n+1} = \Phi \underline{x}_n + .5\Theta[3u_n - u_{n-1}]$

corrector; $\underline{x}_{n+1} = \Phi \underline{x}_n + .5\Theta[u_{n+1} + u_n]$

I4 $\underline{x}_{n+1} = \underline{x}_{n-1} + 2T[Ax_n + Bu_n]$

I5 $y_{n+1} = [2I - T^2M^{-1}K]y_n - y_{n-1} + T^2M^{-1}u_n$

I6 $\ddot{y}_{n+1} = [M+T^2K/6]^{-1}[-Ky_n - TK\dot{y}_n - T^2K\ddot{y}_n/3 + u_n]$

$\dot{y}_{n+1} = \dot{y}_n + T[\ddot{y}_{n+1} + \ddot{y}_n]/2$

$y_{n+1} = y_n + T\dot{y}_n + T^2\ddot{y}_n/3 + T^2\ddot{y}_{n+1}/6$

I7 predictor: integrator I6

corrector: integrator I6 with u_n replaced by u_{n+1}

All of the integrators, with the exception of I6 and I1, were accurate for both examples for the smallest time steps. While the modes identified by I1 and I6 for the smallest time steps are perhaps acceptable, both of these integrators degrade quickly with large time steps. Neither predictor-corrector, I3 and I7, was stable for larger time step sizes than the integrator upon which they were based (I2 and I6) although I7 did improve the accuracy of the flutter root estimate over I6. The flutter mode damping estimates of I5, I6, and I7 show a disconcerting behavior of reversing trends as the time step is increased, whereas the integrators based upon the transition matrix (I1, I2, and I3) give uniform damping estimate degradation. The heavily damped pitch mode of Example 1 is in close agreement with the PHYTRAN2 value for small time steps, whereas the plunge mode damping value for Example 2 which is given by PHYTRAN2 is only one-half the value estimated from the HYTRAN2 results. As the time step

TABLE 4. AEROELASTIC MODES IDENTIFIED FOR EXAMPLE 1 at V = 1.5 and M = 0.8.

a), flutter (plunge) mode

		T,sec.				
Integrator	PHYTRAN2	.0001	.0005	.001	.002	.003
I1	.01+j146.27	.60+j146.59	2.63+j145.77	4.76+j145.35	8.68+j144.18	12.11+j142.65
I2		.12+j146.66	.31+j140.20	.23+j146.54	.33+j147.88	.91+j149.91
I3		.12+j146.65	.28+j146.03	unstable		
I4		.13+j146.66	unstable			
I5		.13+j146.65	.26+j146.13	.00+j146.30	-.69+j147.16	unstable
I6		1.07+j146.52	4.85+j145.37	8.89+j144.30	unstable	
I7		.11+j146.66	.21+j146.07	-.22+j146.01	unstable	

b). pitch mode

I1	-101.32+j498.02	-97.77+j509.73	-108.94+j521.06	-123.91+j534.60	-146.32+j570.70	-154.30+j615.40
I2		-94.78+j507.09	-100.60+j506.28	-113.44+j502.19	-163.45+j503.05	-283.03+j578.20
I3		-94.65+j507.16	-97.10+j507.86	unstable		
I4		-94.57+j507.61	unstable			
I5		-94.50+j507.43	-98.43+j509.75	-107.65+j512.72	-156.20+j528.83	unstable
I6		-99.20+j512.60	-119.17+j547.47	-74.33+j614.32	unstable	
I7		-95.04+j507.37	-98.57+j517.91	-73.18+j549.55	unstable	

TABLE 5. AEROELASTIC MODES IDENTIFIED FOR EXAMPLE 2 AT V = .747 and M = 0.8.

a). flutter (pitch) mode

		T, sec.				
Integrator	PHYTRAN2	.001	.005	.01	.02	.03
I1	.02+j29.57	-.02+j29.37	-.12+j29.23	-.24+j28.99	-.38+j28.37	-.40+j27.78
I2		-.00+j29.43	.00+j29.49	.06+j29.48	.19+j29.22	.28+j28.83
I3		-.01+j29.43	-.03+j29.51	-.08+j29.58	unstable	
I4		-.00+j29.42	.08+j29.89	unstable		
I5		-.00+j29.42	-.01+j29.54	.03+j29.70	.16+j30.08	unstable
I6		-.03+j29.31	-.20+j29.14	-.31+j29.12	.89+j29.45	unstable
I7		-.00+j29.42	-.03+j29.73	.098+j30.55	unstable	

b). plunge mode

I1	-7.46+j25.02	-15.73+j22.31	-15.94+j22.53	-16.40+j22.83	-20.20+j22.40	-28.67+j18.10
I2		-15.40+j22.31	-14.49+j22.34	-13.97+j21.96	-15.00+j20.77	-17.80+j19.06
I3		-15.40+j22.32	-14.36+j22.46	-13.34+j22.45	unstable	
I4		-15.46+j22.35	-11.10+j22.84	unstable		
I5		-15.47+j22.34	-14.58+j22.65	-14.04+j22.68	-14.38+j22.64	unstable
I6		-16.05+j22.21	-17.46+j22.37	-19.50+j23.58	- 9.32+j36.49	unstable
I7		-15.40+j22.24	-14.17+j22.36	-12.59+j22.78	unstable	

was increased, all of the integrators eventually experienced a high frequency instability which could not be attributed to a structural mode instability. Integrators I1 and I2 were unstable for time steps of .004 sec. for Example 1 and .04 sec. for Example 2. At these time steps, the structural integration is being performed with only 3-5 steps per cycle of oscillation of the higher frequency mode. The integrator giving the best overall performance was I2 which gave usable flutter mode damping results for time steps 50% larger than the next best integrator, I5. Integrator I2 was used for the remainder of the study.

Transonic Flutter Analysis

In this section, the techniques demonstrated above are applied to the full nonlinear equation, (1). Flutter boundaries are presented for the structural dynamic model of Example 1 of Table 1 and for NACA 64A010 and MBB A-3 airfoils. Steady-pressure distributions for the ranges of Mach number and angle-of-attack investigated are given in figures 5 and 6. In the cases where the steady shocks are located near the trailing edge, the shock strengths are of concern. For these cases in figures 5 and 6, the computed Mach numbers ahead of the upper surface shocks are only slightly less than 1.3 - the Mach number at which entropy rises start to become signficant indicating that these calculations are on the edge of and possibly outside the range of applicability of TSP theory. At $\alpha = -1.5^{0}$, the Mach number on the lower surface of the MBB A-3 is such that these cases may be beyond the scope of the TSP theory.

Effect of Integration Step Size - The effect of integration step size upon the modes identified from the angle-of-attack response is given in Table 6 for the NACA 64A010 at $M = 0.8$. The flutter speed index is $V_f = 1.07$ and $k_f = 0.139$. A comparison with the Integrator I2 results of Table 4 indicates slightly smaller changes due to step size in the mode estimates for the nonlinear case and gives confidence in the application of the time-marching technique to nonlinear aeroelastic problems.

Table 6. - MODAL ESTIMATES FOR NACA 64A010 AT $M = 0.8$, $\alpha = 0$ DEG., AND $V_f = 1.07$ AS A FUNCTION OF T.

T, sec	s_1, r/s	s_2, r/s
.0001	.11+j115.21	-31.89+j536.26
.0005	.08+j115.09	-32.95+j536.17
.001	.02+j115.18	-35.76+j537.04
.002	-.08+j115.54	-42.03+j544.83
.003	-.07+j116.08	-46.07+j551.90

Effect of Amplitude - The effect of amplitude on the response at flutter was studied for the MBB A-3 airfoil at three conditions: 1)$M = 0.775$ and $\alpha = 0$ deg. where the flow is subcritical, 2)$M = 0.79375$ and $\alpha = 0.5$ deg. where there is a strong shock aft of midchord, and 3)$M = 0.8$ and $\alpha = 0.5$ deg. where the shock is at the trailing-edge. Table 7 gives the modal estimates including the amplitude estimates from the α-fit for $M = 0.775$ which is typical. The flutter speed index is $V_f = 1.21$ and $k_f = 0.125$. There is a surprisingly small effect of amplitude upon the damping of the flutter mode. The damping ratio, ζ, changes from +0.011 for $h_0 = 0.01$ where the oscillation amplitude is +0.28 deg. to -0.004 for $h_0 = 0.10$ where the oscillation amplitude is +2.97 deg. Inspection of the pressure distribution for the $h_0 = 0.1$ case during a cycle of oscillation revealed a complex pattern of shock motion. During a portion of the cycle, a strong shock forms near the 70% chord position, travels forward, weakens, and disappears between 40-50% chord. This is the type B shock motion studied by Tidjeman.[27] Also, during the nose-down portion of the cycle a strong shock forms at 5-10% chord on the lower surface. It is interesting that the modal amplitudes, a_1, are nearly linear with respect to h_0, even for the large amplitudes studied. At $M = 0.79375$ the effect of amplitude upon the flutter mode was smaller than that shown in Table 7, the change in the flutter root in going from $h_0 = 0.01$ to 0.10 being $s = -0.30+j0.69$ rad/sec. At $M = 0.8$ the corresponding change was $s = -1.41-j0.19$. In all cases the standard deviations of the estimates, which did not vary appreciably with h_0, were small and of the order given in Table 1 and the amplitudes varied nearly linearly with h_0. Calculations of amplitude effects were made for the NACA 64A010 and similar small effects on the modal estimates were observed. These results contrast with Dowell et al[28] who studied forced oscillations of the NACA 64A006 airfoil using LTRAN2 and postulated that nonlinear aerodynamics would be important at $k = 0.1$ for oscillatory amplitudes greater than 0.5 degrees. In summary, it appears that, for a given Mach number and steady angle-of-attack, the aeroelastic response of airfoils with dynamics similar to those studied may be treated as locally linear in amplitude within the limits of small disturbance theory.

TABLE 7. MODAL ESTIMATES FOR MBB A-3 AT $M = 0.775$ AND $\alpha = 0$ DEG. AS A FUNCTION OF h_0

h_0	s_1, r/s	s_2, r/s	a_1, deg	a_2, deg
.01	-1.31+j117.17	-46.53+j529.55	.28	.34
.02	-1.26+j117.17	-46.20+j528.77	.60	.66
.04	-1.02+j117.15	-46.48+j528.28	1.21	1.31
.10	.42+j117.24	-48.85+j527.14	2.97	3.24

Comparison of TSP Flutter Boundaries For Example 1 - The transonic flutter boundary of Example 1 with an NACA 64A010 airfoil at $\alpha = 0$ deg. has been studied by Isogai[9,16] using an EXTRAN2 code to obtain harmonic perturbation airloads and by Ehlers and Weatherill[29] using a transonic code, OPTRAN2, to compute the harmonic linear perturbation

studies were then calculated using traditional frequency-domain techniques. The comparison of these flutter boundaries with that obtained from time-marching solutions using HYTRAN2 is shown in figure 7. Also shown are two flutter points at Mach 0.8 and 0.825 which used LTRAN2 aerodynamics. As in figure 4, the LTRAN2 flutter point is conservative by up to 60% in flutter speed index while the HYTRAN2 results are slightly unconservative below M = 0.85 when compared to EXTRAN2. The HYTRAN2 results compare favorably with Isogai's EXTRAN2 results with both giving minimum flutter speed indices of $V_f \approx 0.5$. The HYTRAN2 and EXTRAN2 curves are displaced from each other by M = 0.015 which may be due to differences in steady pressure distribution caused by grid differences. The minimum V_f obtained using HYTRAN2 occurs at M = 0.85 where the steady shock is at x/2b = 0.75. The flutter speed index is slightly greater at M = 0.875 where Isogai was unable to obtain a flutter solution. The OPTRAN2 results (using NACA 64A010A[19] airfoil coordinates) are in reasonable agreement with HYTRAN2 and EXTRAN2 for $M < 0.82$. Multiple flutter points are predicted by OPTRAN2 for Mach numbers above the minimum M_f ($0.85 < M < 0.87$) and the HYTRAN2 calculations have confirmed this effect at M = 0.875. Ref. 29 indicates a complex flutter boundary at larger values of V for $0.88 < M < 0.90$ which has not been studied with HYTRAN2. Thus the flutter boundary between M = 0.875 and M = 0.9 is not shown. For $M > 0.9$ the shock has moved off the trailing-edge and the EXTRAN2 and HYTRAN2 results are in good agreement.

Effect of Angle-of-Attack - The angle-of-attack is known to be an important parameter affecting transonic flutter. Ashley[30] lists several instances of such an effect and Doggett and Ricketts[31] have studied the effect of angle-of-attack upon an arrow-wing configuration. Edwards[32] gives subcritical damping estimates indicating changes in damping ratio of 0.02 for a 0.3 deg increase in angle-of-attack for a supercritical wing. Yates et al[33] give wind tunnel flutter test results of a similar wing at several different angles-of-attack. A novel feature of the flutter boundaries shown is the occurence of multiple flutter speed indices for Mach numbers less than that at the bottom of the transonic dip. That is, as the flutter speed index decreased with increasing Mach number, cases were studied in which further decreases in speed index resulted in the flutter Mach number decreasing also. This curl-back of the flutter boundary occured for angle-of-attack changes of approximately two degrees. Houwink et al[34] report a similar occurrence.

The effects of angle-of-attack upon the flutter boundaries of the NACA 64A010 and MBB A-3 airfoils for Example 1 are shown in figures 8 and 9. Changes in α of 1.5 degrees can induce a 50% drop in V_f for the NACA 64A010 between Mach 0.775 and 0.80 and a 60% drop in V_f for the MBB A-3 between Mach 0.77 and 0.79. The reduced frequencies at flutter for the two examples range from $k_f = 0.12$ for the higher V_f values to $k_f = 0.2$ for the lowest. A key feature is that the boundaries of fig. 8 show a more gradual steepening than those of fig. 9 as Mach number increases. Comparing figs. 6 and 9 indicates that the abrupt steepening of the MBB A-3 boundaries occurs at the Mach number at which the upper surface shock forms. The minimum V_f of both airfoils is approximately 0.5 and is not a strong function of α. Also, the width of the transonic dip near the minimum V_f is greater for the NACA 64A010 than for the MBB A-3, which correlates with the change in Mach number required for the shock to travel from near midchord to the trailing edge (see figs. 5 and 6). For both airfoils, the boundary rises sharply when the shock reaches the trailing edge.

Figure 10 gives the bending mode root locus for the NACA 64A010 versus V for several angles-of-attack and Mach numbers. Fig. 10a presents root loci typical of the case in which the shock has not yet moved aft on the airfoil (see fig. 5). Increasing angle-of-attack causes a loss of damping and a drop in flutter speed index and frequency. Fig. 10b typifies the case in which the shock is near the trailing edge. Minimum values of V_f occur for this condition and over a small range of angle-of-attack there is little effect upon damping or flutter frequency. In fig. 10c, the shock is still further aft and, for the larger values of α, has moved off of the trailing-edge. In this case, the effect of increasing angle-of-attack reverses, with increasing damping resulting for $\alpha > 0.5$ deg. Also, the locus for $\alpha = 0.75$ deg, indicates the cause of the multiple values of flutter boundaries shown in fig. 7. None of these mechanisms appear to address the experimental condition described by Yates et al[33] and Houwink et al[34] in which the flutter boundary was multiple valued for Mach numbers less than that at the bottom of the transonic dip. This observation led to the investigation described in the following section of the effect of aeroelastic twist due to the static pitching moment.

Effect of Static Pitching Moment - In (3), c_{m_0} acts as a preload which is adjusted to maintain the airfoil at a desired steady angle of attack. An alternative viewpoint is adopted in this section by introducing the wind-off angle-of-attack, α_0, and rewriting the static pitching moment equation as

$$k_\alpha(\alpha-\alpha_0) = 1/2\rho U^2(2b)^2 c_m(\alpha, M) \quad (11)$$

which may be reorganized as

$$V^2 = \pi r_\alpha^2 (\alpha-\alpha_0)/2\, c_m(\alpha, M) \quad (12)$$

Equation (12) is a nonlinear equation relating the equilibrium angle-of-attack, α, to the speed index, V, for given values of α_0 and M. With reference to strip-theory type analyses of wings, α_0 may be regarded as a "wing root angle-of-attack" and α as the local section angle-of-attack. The static pitching moment coefficient, $c_m(\alpha)$, is plotted versus α and M for the NACA 64A010 and MBB A-3 airfoils in

figs. 11 and 12. For a given Mach number, the pitching moment curves display three characteristics as α increases: 1)A range of α in which c_m varies relatively linearly with α which corresponds to the transition from shockless flow to flow with mild shocks (see figs. 5 and 6), 2)a range of α in which c_m rises steeply corresponding to strong shocks moving aft on the airfoil, and 3)a range in which c_m again varies linearly with α with a slope which is independent of M corresponding to supersonic flow over the upper surface of the airfoil. Note particularly that the slope of the c_m curve in the first region varies gradually for the symmetrical NACA 64A010 with both M and α whereas the slope of the c_m curve for the supercritical MBB A-3 is almost independent of M and α in this region.

Figures 8 and 9 give flutter boundaries as a function of α. In order to determine flutter boundaries as a function of α_0, taking into account twisting due to the steady pitching moment, the data from figs. 8 and 9 were cross-plotted versus α for fixed M and solutions of (12) superimposed. Figures 13 and 14 give such plots for the NACA 64A010 at M = .8 and the MBB A-3 at M = .775. Intersections of the solution of (12) for a given α_0 with the flutter boundary curve represent flutter points at the indicated value of α. Figure 13 is typical for the NACA 64A010 in that only one flutter point occurs for each value of α_0. In contrast, fig. 14 shows that the MBB A-3 has three flutter points for a range of α_0 near 4 deg. This occurs due to the steeper slope of the flutter boundary curves of the MBB A-3 coupled with the pitching moment behavior shown in fig. 12.

Figures 15 and 16 present the effect of static pitching moment upon the flutter boundary of the two airfoils for $2^0 < \alpha_0 < 5^0$. Comparing figs. 8 and 15, the effect for the NACA 64A010 is to steepen the flutter boundaries for Mach numbers between M = 0.75 and 0.8. Comparing Figs. 9 and 16, the effect for the MBB A-3 is much more pronounced. Multiple flutter points for a given Mach number cause the flutter boundary to curl back as V is decreased for α_0 > 3 deg. The amount of the curl-back in flutter Mach number is similar to that shown in ref. 33. At α_0 = 4 deg. M_f decreases 0.025 as V_f decreases from 1.1 to 0.65. The flutter boundaries shown in figs. 15 and 16 for V_f < 0.8 correspond to Mach number and angle-of-attack combinations in which the shock has moved aft on the airfoil. In these cases, unmodeled boundary layer effects are probably important. Nevertheless, the similarity of the flutter boundary curl back seen in fig. 16 to those shown in refs. 33 and 34 indicates that static aeroelastic twisting can have a significant effect upon transonic flutter.

The multiple valued flutter curves shown in fig. 16 have an interesting interpretation in terms of flutter testing. At M=0.775 and α_0 = 3 deg., the bending mode root locus as a function of speed index is shown in fig. 17. The speed index, V, and actual angle-of-attack, α, are noted along the locus and show that the airfoil is twisted nose down as V is increased. Shown near V = 0.6 and α = 1 deg. is a local minimum in damping due to the proximity to the α_0 = 3 deg flutter boundary shown in fig. 16. As V increases, the mode becomes damped again and finally flutters at V_f = 1.3 where α = -0.7 deg. A small increase in either M or α_0 would lead to flutter at V_f = 0.6. The flutter point at ω = 133 rad/sec corresponds to a classical type of flutter in which significant frequency coalescence occurs. The incipient flutter condition at ω = 85 rad/sec has much less frequency coalescence and is similar to cases which have been termed "single degree of freedom" or "shock induced" flutter.[30] Inspection of the static pressure distributions corresponding to these two conditions in fig. 6 indicates that the lower frequency flutter occurs when a shock has developed on the upper surface.

Concluding Remarks

The transonic small perturbation equation has been coupled with the structural equations of motion of a pitching and plunging airfoil and time-marching transient flutter solutions have been obtained. Accurate frequency and damping estimates were obtained by means of a complex exponential least squares curve fit of the responses. The accuracy of the time-marching calculations was established by comparison of results from the linearized transonic equation and by comparison of the flutter boundary obtained with the nonlinear equation with published results. Seven candidate numerical integration algorithms for the structural equations were evaluated. The preferred algorithm is a modified state transition matrix integrator which was more accurate and stable for larger time steps than the others.

The flutter boundaries of symmetrical NACA 64A010 and supercritical MBB A-3 airfoils were determined for an example demonstrating a pronounced transonic dip. Comparison of flutter boundaries calculated using several nonlinear transonic aerodynamic codes show good agreement in predicting the transonic dip. The response at flutter was surprisingly linear in amplitude for angle-of-attack oscillations of up to three degrees. The effect of angle-of-attack upon the flutter boundaries of the two airfoils was determined. Changes of 1.5 deg in angle-of-attack can cause a 50% decrease in flutter speed index for the NACA 64A010 and a 60% decrease for the MBB A-3. The slope of the flutter boundary with Mach number is larger for the MBB A-3 airfoil and appears to correlate with steady shock strength and locations on the airfoil. When aeroelastic twisting due to the static pitching moment is included, the steeper flutter boundary of the MBB A-3 leads to the occurrence of multiple flutter points for a given Mach number and a situation in which the flutter boundary Mach number decreases as speed index is decreased. This effect has been observed in flutter model tests.

References

[1]Ballhaus, W. F. and Goorjian, P. M., "Implicit Finite-Difference Computations of Unsteady Transonic Flow About Airfoils," AIAA Journal, vol. 15, no. 12, Dec. 1977.

[2]Ballhaus, W. F., and Goorjian, P.M., "Computation of Unsteady Transonic Flows by the Indicial Method." AIAA Journal, vol. 16, Feb. 1978.

[3]Rizzetta, D. P., "Time-Dependent Response of a Two-Dimensional Airfoil in Transonic Flow," AIAA Journal, vol. 17, no. 1, January 1979.

[4]Yang, T. Y., Guruswamy, P., and Striz, A. G., "Aeroelastic Response Analysis of Two-Dimensional, Single and Two Degree of Freedom Airfoils in Low-Frequency, Small Disturbance Unsteady Transonic Flow," AFFDL-TR-79-3077, June 1979.

[5]Yang, T. Y., Guruswamy, P., and Striz, A. G., "Flutter Analysis of a Two-Dimensional and Two-Degree-of-Freedom Supercritical Airfoil in Small-Disturbance Unsteady Transonic Flow," AFWAL-TR-80-3010, March 1980.

[6]Traci, R. M., Albano, E. D., and Farr, J. L., Jr., "Perturbation Method for Transonic Flows About Oscillating Airfoils," AIAA Journal, vol. 14, no. 9, Apr. 1976.

[7]Houwink, R., and van der Vooren, J., "Improved Version of LTRAN2 for Unsteady Transonic Flow Computations," AIAA Journal, vol. 18, no. 8, Aug. 1980.

[8]Rizzetta, D. P., and Chin, W. C., "Effect of Frequency in Unsteady Transonic Flow," AIAA Journal, vol. 17, no. 7, July 1979.

[9]Isogai, K., "Transonic Dip Mechanism of Flutter of a Sweptback Wing: Part II," AIAA Journal, vol. 19, no. 9, Sept. 1981.

[10]Borland, C. J., and Rizzetta, D. P., "Nonlinear Transonic Flutter Analysis," Paper No. AIAA-81-0608-CP, AIAA Dynamic Specialist Conference, Atlanta, GA, April 1981.

[11]Engquist, B., and Osher, S., "Stable and Entropy Satisfying Approximations for Transonic Flow Calculations," Mathematics of Computations, vol. 14, 1980, pp. 45-75.

[12]Bland, S. R., "Development of Low Frequency Kernel-Function Theory and Comparison with Time-Dependent Finite-Difference Methods," NASA TM 83283, 1982.

[13]Goorjian, P. M. and Van Buskirk, R., "Implicit Calculations of Transonic Flows Using Monotone Methods," AIAA Paper No. 81-0331, AIAA Aerospace Sciences Meetings, St, Louis, MO, 1981.

[14]Brockett, R. , "Finite Dimensional Linear Systems," John Wiley and Sons, Inc., 1970.

[15]Edwards, J. W., "A FORTRAN Program for the Analysis of Linear Continuous and Sampled-Data systems," NASA TM X-56038, Jan. 1976.

[16]Isogai, K., "Numerical Study of Transonic Flutter of a Two-Dimensional Airfoil,"National Aerospace Laboratory, Japan, TR-617T, July 1980.

[17]Bennett, R. M., and Desmarais, R. N., "Curve Fitting of Aeroelastic Transient Response Data with Exponential Functions in Flutter Testing Techniques," NASA SP-415, 1975, pp. 43-58.

[18]Abbott, I. H., and von Doenhoff, A. E., "Theory of Wing Sections," Dover, 1959.

[19]Bland, S. R., "AGARD Two-Dimensional Aeroelastic Configurations," AGARD Advisory Report No. 156, 1980.

[20]Rizzetta, D. P., and Yoshihara, H., "Computation of the Pitching Oscillation of a NACA 64A010 Airfoil in the Small Disturbance Limit," AIAA Paper No. 80-128, AIAA Aerospace Sciences Meeting, Pasadena, CA, Jan. 1980.

[21]Yang, T. Y., Guruswamy, P., and Striz, A. G., "Application of Transonic Codes to Flutter Analysis of Conventional and Supercritical Airfoils," AIAA Paper No. 81-0603, AIAA Structures, Structural Dynamics, and Materials Conference, Atlanta, GA, April 1981.

[22]Yang, T. Y., and Chen, C. H.,"Flutter and Time Response Analysis of Three Degree of Freedom Airfoils in Transonic Flow," AFWAL-TR-81-3103, August 1981.

[23]Bucciantini, G., Oggiano, M. S., and Onorato, M., "Supercritical Airfoil MBB A-3 Surface Pressure Distributions, Wake and Boundary Condition Measurements in Experimental Data Base for Computer Program Assessment," AGARD AR-138, 1979.

[24]Olsen, J. J., "AGARD Standard Configurations for Aeroelastic Applications of Transonic Unsteady Aerodynamics, Part III, Candidate Airfoil Data," AFFDL-TM-78-6-FBR, Air Force Flight Dynamics Lab., January 1978.

[25]Edwards, J. W., "Applications of Laplace Transform Methods to Airfoil Motion and Stability Calculations," AIAA Paper No. 79-0772, AIAA Structures, Structural Dynamics, and Materials Conference, St. Louis, MO, May 1979.

[26]Borland, C. J., and Rizzetta, D. P., "Transonic Unsteady Aerodynamics for Aeroelastic Applications, Vol. I - Technical Development Summary," AFWAL-TR-80-3107, May 1981.

[27]Tidjeman, H., "Investigations of the Transonic Flow Around Oscillating Airfoils," National Aerospace Laboratory, The Netherlands, NLR TR 77090 U, 1977.

[28]Powell, E. H., Bland, S. R, and Williams, M. H., "Linear/Nonlinear Behavior in Unsteady Transonic Aerodynamics," AIAA Paper No. 81-0643, AIAA Dynamics Specialists Conference, Atlanta, GA, April 1981.

[29]Ehlers, F, and Weatherill W., "A Harmonic Analysis Method for Unsteady Transonic Flow and Its Application to the Flutter of Airfoils," NASA CR 3537, 1982.

[30]Ashley, H., "The Role of Shocks in the "Sub-Transonic" Flutter Phenomenon," Journal of Aircraft, Vol. 17, no. 3, March 1980, pp. 187-197.

[31]Doggett, R. V., Jr., and Ricketts, R. H., "Effects of Angle-of-Attack and Ventral Fin on Transonic Flutter Characteristics of an Arrow-Wing Configuration," NASA TM 81914, December 1980.

[32]Edwards, J. W., "Flight Test Results of an Active Flutter Suppression System Installed on a Remotely Piloted Research Vehicle," NASA TM 83132, May 1981 (also AIAA Paper No. 81-0655).

[33]Yates, E. C., Jr., Wynne, E. C., and Farmer, M. G., "Measured and Calculated Effects of Angle of Attack on the Transonic Flutter of a Supercritical Wing," AIAA Paper No. 82-0647, AIAA Structures, Structural Dynamics, and Materials Conference, New Orleans, La, May 1982.

[34]Houwink, R., Kraan, A. N., and Zwaan, R. J., "A Wind-Tunnel Study of the Flutter Characteristics of a Supercritical Wing," AIAA Paper No. 81-0651, AIAA Dynamics Specialists Conference, Atlanta, GA, April 1981.

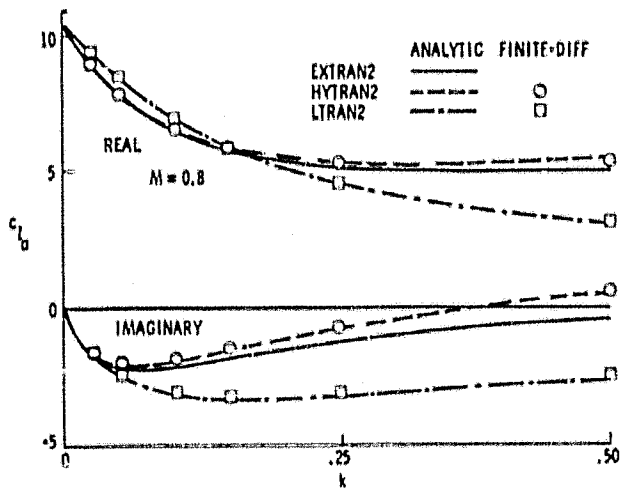

Fig. 1 Comparison of analytic and finite-difference calculations of lift coefficient due to pitching oscillation about midchord.

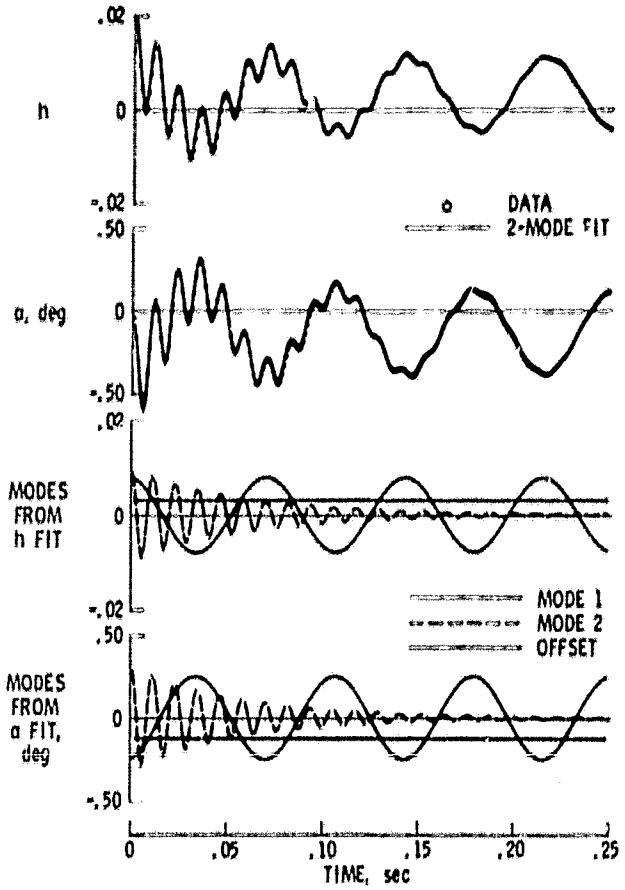

Fig. 2 Fit of transient response of MBB A-3 airfoil at M = 0.8, α = 0 deg., and V_f = 0.645 for Example 1.

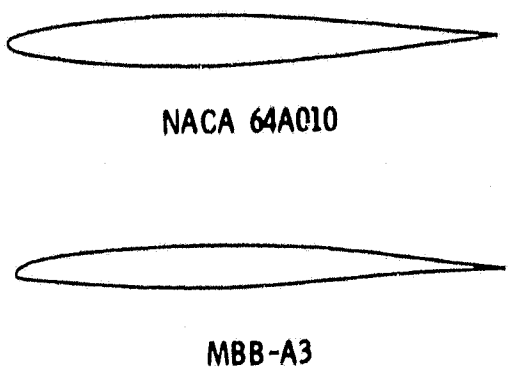

Fig. 3 Airfoil profiles.

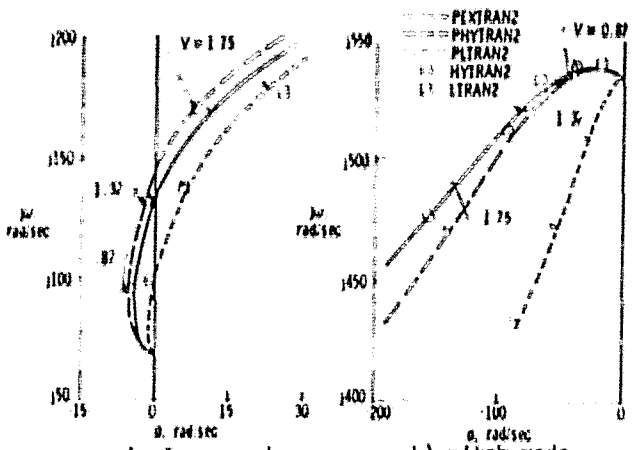

a) plunge mode b) pitch mode

Fig. 4 Comparison of linearized root loci for Example 1 at M = 0.8.

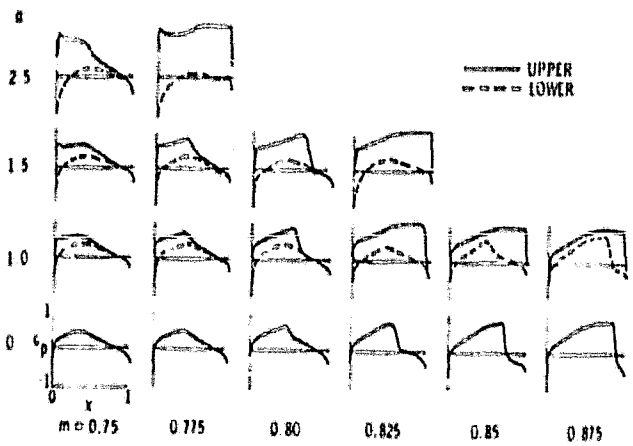

Fig. 5 NACA 64A010 steady pressure distributions as a function of Mach number and angle-of-attack.

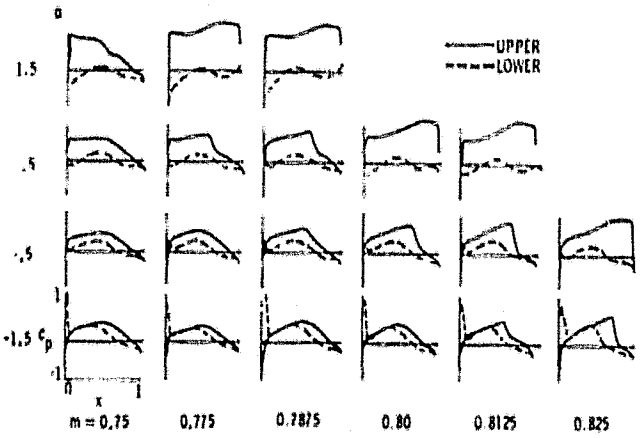

Fig. 6 MBB A-3 steady pressure distributions as a function of Mach number and angle-of-attack.

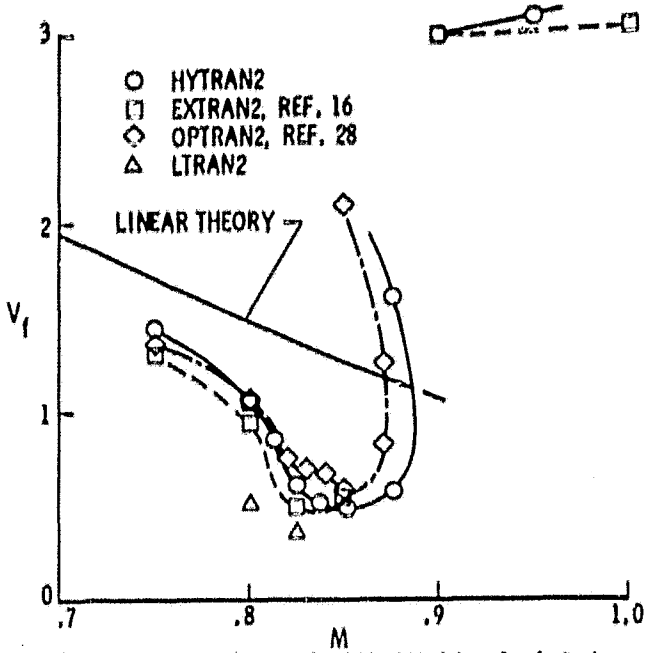

Fig. 7 Comparison of NACA 64A010 calculated flutter boundaries.

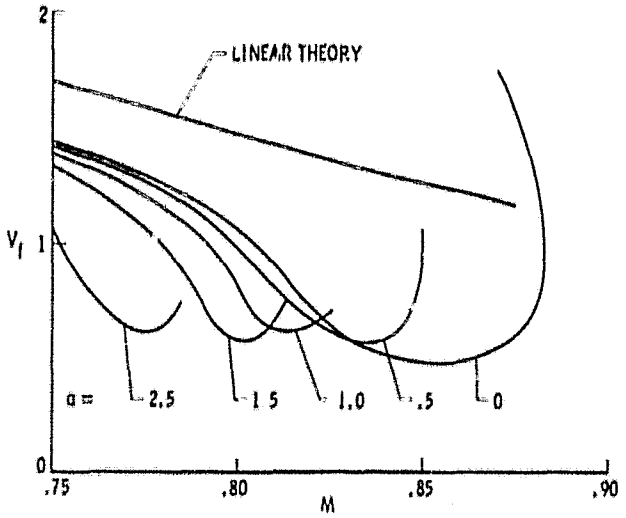

Fig. 8 Effect of angle-of-attack upon NACA 64A010 flutter boundaries obtained from HYTRAN2.

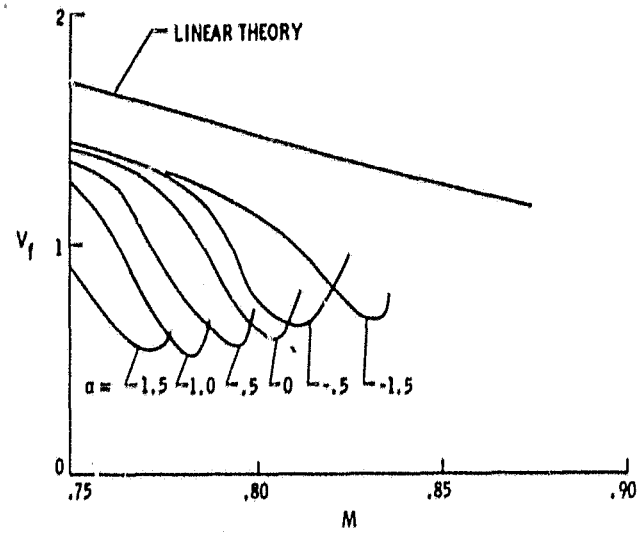

Fig. 9 Effect of angle-of-attack upon MBB A-3 flutter boundaries obtained from HYTRAN2.

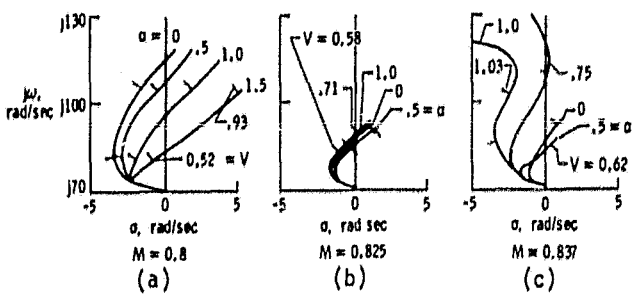

Fig. 10 NACA 64A010 flutter mode root locus as a function of M, V, and angle-of-attack.

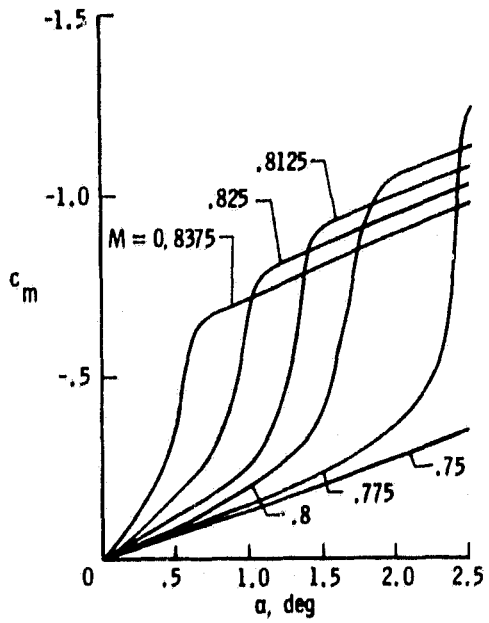

Fig. 11 Static pitching moment of NACA 64A010 about x/b = -2 as a function of Mach number and angle-of-attack.

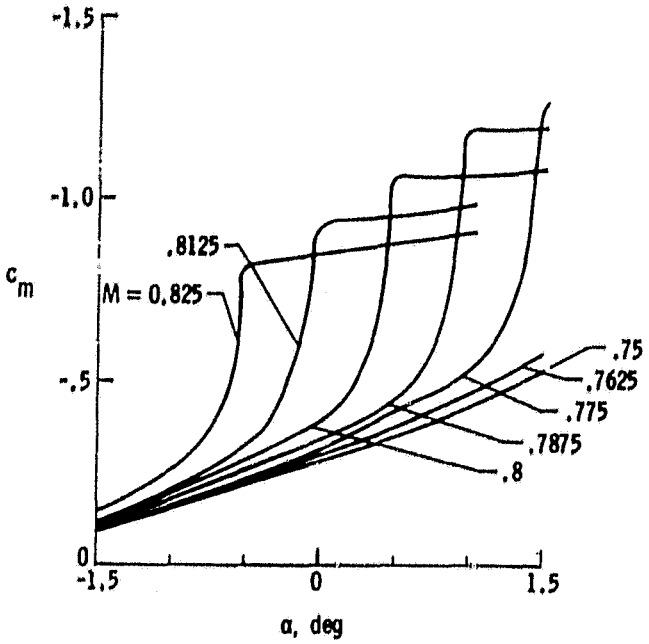

Fig. 12 Static pitching moment of MBB A-3 about x/b = -2 as a function of Mach number and angle-of-attack.

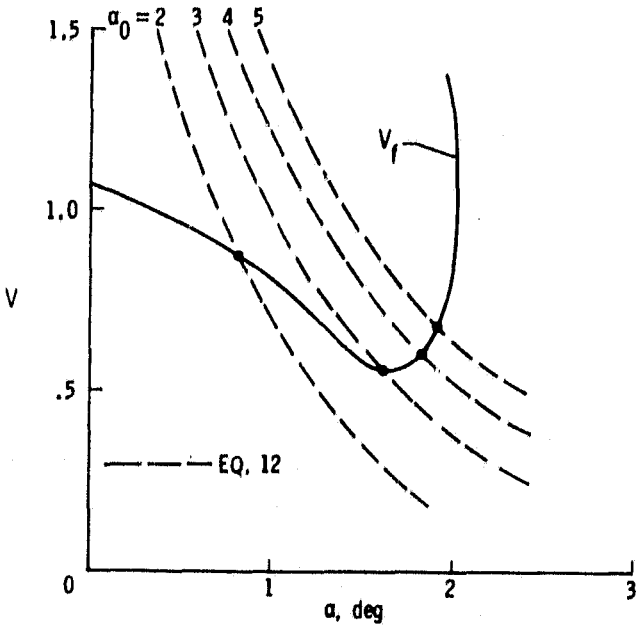

Fig. 13 Graphical determination of NACA 64A010 flutter conditions at M = 0.8 including effect of static pitching moment.

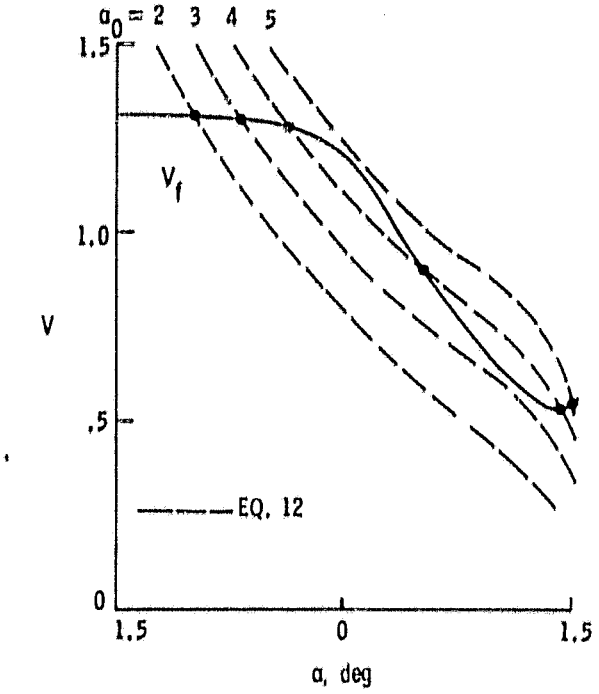

Fig. 14 Graphical determination of MBB A-3 flutter conditions at M = 0.775 including the effect of static pitching moment.

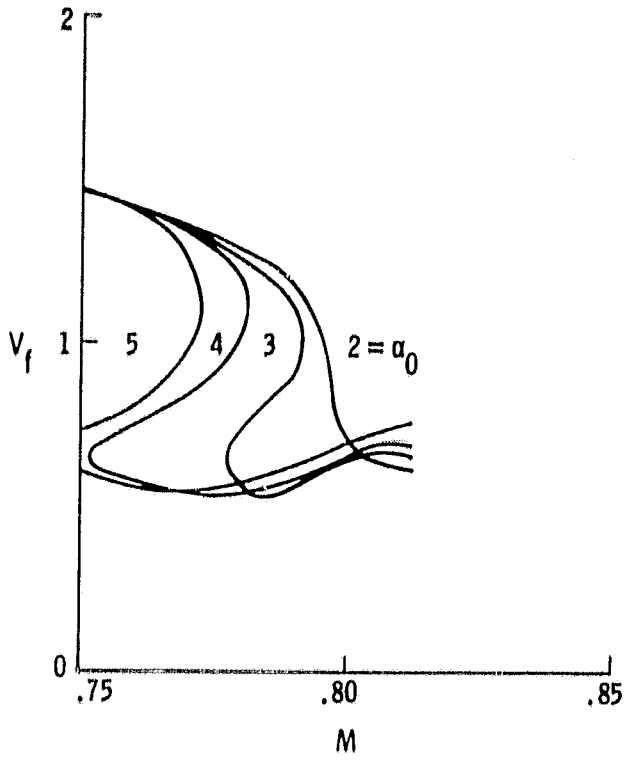

Fig. 16 The effect of static pitching moment on MBB A-3 flutter boundaries.

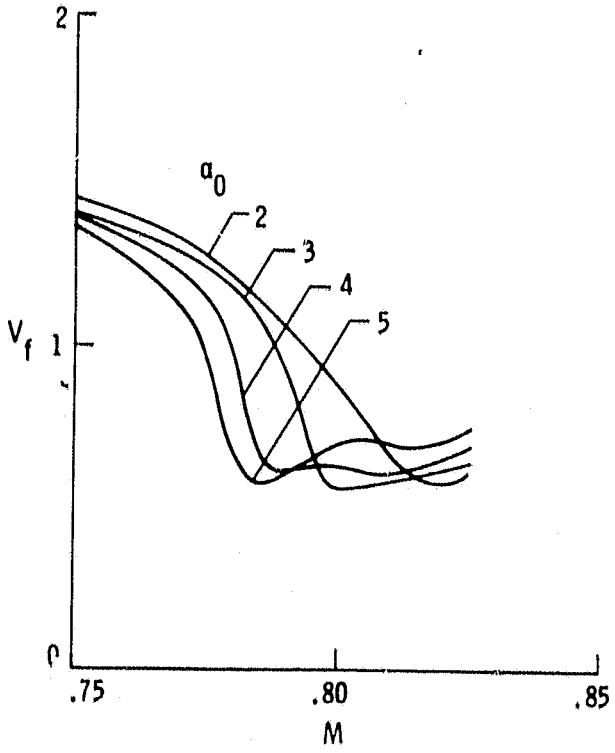

Fig. 15 The effect of static pitching moment on NACA 64A010 flutter boundaries.

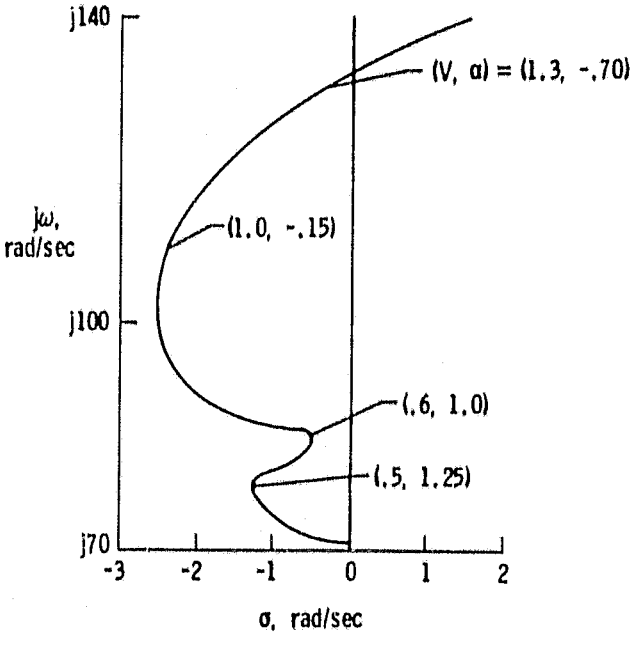

Fig. 17 MBB A-3 flutter mode root locus vs. V for α_0 = 3 deg. and M = 0.775.